Electronic Supplementary Material (ESI) for Journal of Materials Chemistry C.

Supplementary Information

Color Controllable Smart White Lighting based on Various Device Architectures of Electrically-Driven Quantum-Dot Light-Emitting Diodes

Dong-Wook Shin, Sanghyo Lee, Hyung Woo Choi, Sang Yun Bang, Soo Deok Han, Yul Jae Cho, Xiang-Bing Fan, Jeong-Wan Jo, Limeng Ni, Chatura Samarakoon, Adrees Arbab, Jiajie Yang, Yoonwoo Kim, Sung-Min Jung,* Luigi G. Occhipinti, Gehan A. J. Amaratunga, and Jong Min Kim*

Electrical Engineering Division, Department of Engineering, University of Cambridge, 9 JJ Thomson Avenue, Cambridge, CB3 0FA, United Kingdom

E-mail: sj569@cam.ac.uk and jmk71@cam.ac.uk

Charge transport model in QD-LED device

The injection current densities of J_p^i and J_n^i are described by an electric-field dependent carrier capturing process between the QD layer and charge transport layers. In this study, the subscripts p and n denote the hole and electron. The injection current densities are expressed as Eq. (S1).[1]

$$J_p^i = q\alpha_p\mu_p^{QD}F_pT_p^{BI}p_h\left(N_{QD} - p_{QD}\right),$$
$$J_n^i = -q\alpha_n\mu_n^{QD}F_nT_n^{BI}n_e\left(N_{QD} - n_{QD}\right). \quad \text{(S1)}$$

Here, q is the electric charge of a proton. α's are capturing volume for the given QDs and μ^{QD}'s are the mobilities of respective carriers in QD layer. F's are the electric field intensities acting on the respective carriers at the interfaces between QD and transport layers. T^{BI}'s are injection tunnelling probabilities of the respective carriers for the energy barrier from the transport layers to the shell of the QDs. The hole and electron densities at the HTL and ETL surfaces facing QD layer are given by p_h and n_e, respectively. p_{QD} and n_{QD} are the hole and electron densities at the center of the QDs adjacent to the HTL and ETL, and N_{QD} is the density of QDs calculated by $N_{QD} = (3/4\pi)\times(d_{QD}/2)^{-3}$ where d_{QD} is the diameter of the QDs.

The drift-diffusion current densities in the transport layers, J_p^d and J_n^d, are described by summation of the drift and diffusion current densities as expressed in Eq. (S2).[2,3]

$$J_p^d = q\mu_p pF_p - \mu_p k_B T\frac{\partial p}{\partial z},$$
$$J_n^d = q\mu_n nF_n + \mu_n k_B T\frac{\partial n}{\partial z}. \quad \text{(S2)}$$

Here, μ's are the carrier mobilities in the given transport layers, F's are the aforementioned electric field intensities at a given position in the transport layers. k_B and T are the Boltzmann constant and the absolute temperature of the device. The hole and electron mobilities for the given transport layers are listed in Table S1.

For the hopping current, the energy level difference and its electric-field effect on the charge transport between QDs are also considered by including the electric field-dependent charge carrier capturing process together with the Boltzmann tunnelling process. The hopping current densities, $J_{\mathrm{p}}^{\mathrm{h}}$ and $J_{\mathrm{n}}^{\mathrm{h}}$ from the m-th QD to (m+1)-th QD, are expressed as Eq. (S3).[1,4]

$$\begin{aligned} J_{\mathrm{p}}^{\mathrm{h}} &= q v_{\mathrm{p}}^{\mathrm{th}} T_{\mathrm{p}}^{\mathrm{BH}} \left(B_{\mathrm{p}}^{m \to m+1} p_m^{\mathrm{QD}} - B_{\mathrm{p}}^{m+1 \to m} p_{m+1}^{\mathrm{QD}} \right) \\ &\quad + q \alpha_{\mathrm{p}} \mu_{\mathrm{p}}^{\mathrm{QD}} F_{\mathrm{p}} T_{\mathrm{p}}^{\mathrm{BH}} p_m^{\mathrm{QD}} \left(N_{m+1}^{\mathrm{QD}} - p_{m+1}^{\mathrm{QD}} \right) \\ J_{\mathrm{n}}^{\mathrm{h}} &= -q v_{\mathrm{n}}^{\mathrm{th}} T_{\mathrm{n}}^{\mathrm{BH}} \left(B_{\mathrm{n}}^{m \to m+1} n_m^{\mathrm{QD}} - B_{\mathrm{n}}^{m+1 \to m} n_{m+1}^{\mathrm{QD}} \right) \\ &\quad - q \alpha_{\mathrm{n}} \mu_{\mathrm{n}}^{\mathrm{QD}} F_{\mathrm{n}} T_{\mathrm{n}}^{\mathrm{BH}} n_{m+1}^{QD} \left(N_m^{\mathrm{QD}} - p_m^{\mathrm{QD}} \right) \end{aligned} \tag{S3}$$

Here, v^{th}'s and $B^{\mathrm{a}\to\mathrm{b}}$'s are the thermal velocities of carriers and Boltzmann probabilities for the carriers hopping from a to b QDs.[5] T^{BH} in Eq. (S3) is the tunnelling probability of the energy barriers between two QDs during the carrier hopping process. In the case of the monochromatic QD-LEDs, the electric-field-dependent carrier capturing volume of the hole and electron, α_{p} and α_{n}, are set to be zero to neglect the carrier capturing process within the homogeneous QD layer. In the stacked QD-LEDs, since the EML is composed of heterogeneous QD layer, the hole capturing volumes α_{p} between R and G QDs and between G and B QDs are set to be 4.1×10^{-12} cm^3 and 2.7×10^{-12} cm^3, respectively, and all the electron capturing volumes α_{n} are set to be zero in the simulation of R/G/B and B/G/R stacked QD-LED devices. All the material parameters of the R, G, and B QDs used in the simulation of the patterned-type QD-LED devices is listed in Table S2.

The electric-fields in Eqs. (S1)-(S3) are calculated by the gradient of the energy-level distribution of hole and electron across the device. The energy-level distribution is the summation of the flat-band energy-level of the carriers and the potential distribution which is solved by the Poisson's equation. for the given carrier densities and the boundary conditions of a bias voltage configuration. In order to solve the dynamic behaviors of the hole and electron in the QD-LED devices, the continuity equations are used for the governing equations of the computational modelling.[1–4,6,7] The Poisson's equation is used for solving the electrostatic potential coupled with the continuity equations. The finite different method (FDM) has been utilized as a numerical technique for solving the second-order partial differential equations of

the continuity equations combined with the Poisson's equation on a discretized grid space across the QD-LED device.[8]

The bimolecular radiative recombination rate U_{RAD} at the centers of the QDs is calculated from Eq. (S4) with the simulated distributions of the hole and the electron densities at the centers of QD layers.

$$U_{\mathrm{RAD}} = \gamma(p^{\mathrm{QD}} n^{\mathrm{QD}} - n_i^2) \tag{S4}$$

Here, γ is the Langevin radiative recombination strength which is defined as $\gamma = q(\mu_{\mathrm{p}}^{\mathrm{QD}}+\mu_{\mathrm{n}}^{\mathrm{QD}})/(\varepsilon_{\mathrm{r}}^{\mathrm{QD}}\varepsilon_0)$ with the hole and electron mobilities $\mu_{\mathrm{p}}^{\mathrm{QD}}$ and $\mu_{\mathrm{n}}^{\mathrm{QD}}$, dieletric constant of the QD layer $\varepsilon_{\mathrm{r}}^{\mathrm{QD}}$ and the vacuum permittivity ε_0. In the simulation, γ is set to be 1.0×10^{-12} cm^3 s^{-1} for $\mu_{\mathrm{p}}^{\mathrm{QD}} = \mu_{\mathrm{n}}^{\mathrm{QD}} = 2.6\times10^{-6}$ cm^2 V^{-1} s^{-1} and $\varepsilon_{\mathrm{r}}^{\mathrm{QD}} = 9.4$. n_i is an intrinsic carrier concentration of the QD core material (Table S2). The Shockley-Read-Hall (SRH) recombination rate U_{SRH} and the Auger recombination rate U_{AUG} at the centers of the QDs are also used for non-radiative recombination processes in the device as shown in Eqs. (S5) and (S6).[2,7]

$$U_{\mathrm{SRH}} = \frac{pn - n_{\mathrm{i}}^2}{\tau(p+n)} \tag{S5}$$

$$U_{\mathrm{AUG}} = C(p+n)(pn - n_{\mathrm{i}}^2) \tag{S6}$$

Here, τ is the SRH recombination lifetime and C is the Auger capture probability, respectively.

The EQE of the device under a given bias condition is calculated from the simulated radiative and non-radiative recombination rates at each of the QD center. By integrating the recombination rates U over the entire region of the QD-LED device, the recombination rate per unit area R for the Langevin radiative recombination, the SRH and Auger non-radiative recombination rates can be calculated. Finally, the EQE of the QD-LED device can be obtained by Eq. (S7) with the PLQY of QD layer η_{QD} and the light extraction efficiency η_{E}. Here, η_{QD} is considered to be 0.6 to include the imperfect layer efficiency caused by any exciton quenching sources such as Förster resonant energy transfer (FRET), and η_{E} is set to be 0.2 for the optical

structure of the device.

$$EQE = \frac{\eta_{\mathrm{QD}} \times \eta_{\mathrm{E}} \times R_{\mathrm{RAD}}}{R_{\mathrm{RAD}} + R_{\mathrm{SRH}} + R_{\mathrm{AUG}}} \quad \text{(S7)}$$

For a given Langevin radiative recombination strength γ, the PLQY of the QD layer η_{QD}, the SRH recombination lifetime τ, and the Auger capture probability C are determined to match the simulated EQE-current density curves to the experimental EQE-current density curves of the fabricated QD-LED devices.

Spectral radiances

The spectral radiance of the monochromatic QD-LED device is calculated from the radiative recombination rate per unit area R_{RAD} of the device. For the given peak wavelength λ_{peak}, the spectral radiance $S(\lambda, \lambda_{\mathrm{peak}})$ is obtained from Eq. (S8) with the assumption of the Gaussian distribution for wavelength λ.

$$S(\lambda, \lambda_{\mathrm{peak}}) = A \exp\left[-\frac{4 \ln 2}{\Delta\lambda^2}\left(\lambda - \lambda_{\mathrm{peak}}\right)^2\right] \quad \text{(S8)}$$

Here, A is the peak radiance of the QD-LED device under a given applied voltage and $\Delta\lambda$ is the full width at half maximum (FWHM) of the given QD-LED device. In the simulation, the FWHMs of R, G, and B QDs are equally set to be 20 nm for the simplicity of calculation. A is expressed as Eq. (S9) with the PLQY of the QD layer and η_{QD}, and the radiative recombination rate per unit area R_{RAD}.

$$A = \frac{2\sqrt{\ln 2}}{\Delta\lambda\pi\sqrt{\pi}} \frac{hc}{\lambda_{\mathrm{peak}}} \times \eta_{\mathrm{QD}} \times \eta_{\mathrm{E}} \times R_{\mathrm{RAD}} \quad \text{(S9)}$$

Here, c is the speed of light. Then, the total spectral radiance $L(\lambda)$ of the white lighting system with the set of weighting factors for the R, G, and B pixelated QD-LED patterns is obtained from Eq. (1) by a weighted summation of individual spectrum $S(\lambda, \lambda_{peak})$.

Thermal velocity of carrier in a QD core

When the tunnelling process is taken into account for the hopping current density between two QDs, the thermal velocities of the hole and the electron is used.[1,4] The thermal velocities of the hole and electron in a QD core are expressed by Eq. (S10).

$$v_{\mathrm{p,n}}^{th} = \sqrt{\frac{2k_B T}{m_{\mathrm{p,n}}^*}} \tag{S10}$$

Here, the subscriptions p and n denote the hole and the electron. k_B and T are the Boltzmann constant and the absolute temperature. $m_{\mathrm{p,n}}^*$ are effective masses of the hole and the electron, respectively.

Tunnelling probability of an energy barrier

When a carrier crosses a tunnelling barrier formed by a QD shell of thickness t_s, the tunnelling probability is described as Eq. (S11).[9]

$$T^{\mathrm{B}} = \begin{cases} 1, & \Delta E < 0 \\ \exp\left(-\frac{2\pi}{h} t_s \sqrt{8 m_s^* \Delta E}\right), & \Delta E \geq 0 \end{cases} \tag{S11}$$

Here, ΔE is the energy barrier height defined by $\Delta E = E^{\mathrm{B}} - E$, where E^{B} and E are the energy-levels of the barrier and the carrier, respectively. h is the Planck's constant and m_s^* is the effective mass of the carrier in the QD shell. t_s is the thickness of QD shell and assumed to be 0.25 nm in this study. The tunnelling probability can be used for the calculation of the tunnelling barriers of QD shells for injection current density at the interfaces between charge transport

layers and QD layer, and the calculation of tunnelling barriers of QD shells for the tunnelling and capturing current densities between two neighbouring QDs.

Boltzmann probability for carrier hopping between two QDs

When the energy levels of two QDs are taken into account for calculating the tunnelling current density, the Boltzmann factor is used as the probability of carriers hopping between two energy levels of the neighbouring QDs. The Boltzmann factor for the carrier hopping from one QD denoted by 'a' to another QD denoted by 'b' can be calculated by Eq. (S12).[5]

$$B^{\mathrm{a}\to\mathrm{b}} = \exp\left(-\frac{\Delta E^{a\to b}}{k_{\mathrm{B}}T}\right) \tag{S12}$$

Here, $\Delta E^{\mathrm{a}\to\mathrm{b}}$ is the step height of energy levels between QD a to QD b.

Fabrication of QD-LEDs

The layers of anode (ITO), HIL (PEDOT:PSS), HTL (TFB), EML, ETL (MZO), and cathode (Al) are formed on the glass substrate in the order. For the device fabrication, we used commercially available HIL (PEDOT:PSS Al 4083 from Heraeus), HTL (TFB from Ossila). MZO nanoparticles with 12% mol% of magnesium were prepared by in-house synthesize. The CdSe/ZnS core/shell QDs are purchased from Mesolite ltd. The patterned ITO glass substrates for anode electrode were purchased from Ossila and cleaned by ultrasonication in the acetone and isopropanol, and then treated with oxygen plasma for 5 minutes. The PEDOT:PSS for HIL was spin-coated on the cleaned ITO glass substrate at 4,000 revolutions per minute (rpm) for 30 seconds and annealed at 150 ℃ for 30 minutes under ambient conditions. Subsequently, transferring in the nitrogen-filled glove box, TFB (8 mg ml^{-1} in chlorobenzene) for HTL was spin-coated at 2,000 rpm for 30 seconds and baked at 130 ℃ for 30 minutes. Next, to form the EML, the QD solutions were drop-casted with 4,000 rpm for 30 seconds for mixed- and stacked-types of QD-LEDs. For the transfer printing process, QD layers were coated on donor substrate with the coating condition and transferred on the TFB surface, followed by annealing process at 110 ℃ for 15 minutes. The MZO nanoparticles in ethanol (25 mg ml^{-1}) were spin-

coated at 2,000 rpm for 30 seconds, then annealed at 90 ℃ for 15 minutes. Finally, the Al electrode (200nm) was deposited by the thermal evaporator under 1×10^{-6} Torr.

For patterned-type QD-LED, the electrodes and charge transport layers are fabricated by the same methods as for the other modes. The detailed fabrication process via transfer printing with the donor substrate and patterned PDMS stamp are included in the Supporting Information. For the stacking mode, each of the R, G, and B QD solution in hexane was vertically drop-casted with the same coating conditions. At each step of the spin-coating, each R, G, and B QD layers were annealed at an optimal temperature of 110 ℃ in the glove box to minimize the interfacial mixing and damage to the underlying layer caused by organic solvent, as optimized in Fig. S9. For the mixed-type QD-LED, the fabrication of QD-LEDs starts with preparing mixing QD solutions under same solvent of hexane (12.5 mg ml^{-1}). After mixing R, G, B QD solution in one vial, the mixture solution was stirred for 1 hour without heat for spin-coating process.

Preparation of the donor substrate for transfer printing

The donor substrate has been prepared prior to start fabrication the samples. Cleaned silicon (Si) substrate has been exposed to oxygen plasma to active OH bonds on the substrate, and then placed onto the wet-bath solution for a self-assembly monolayer (SAM) using Octadecyltrichlorosilane (ODTS) (Fig. S10a). Wet-bath solution was made of 30 ml of anhydrous Hexane and 1 ml of ODTS and stirred for 5 minutes. The resulting substrates were rinsed with anhydrous Hexane for 10 minutes to remove unbonded surplus ODTS, and then placed on hot plate and baked at 65 ℃ for 5 minutes to enhance covalent bonding. The SAM acts as a buffer layer between the QDs and silicon and helps in the peeling off the QDs by reducing the surface energy on silicon. Finally, prepared donor substrate was spin-coated using Hexane-based red-green-blue QD precursor independently. The final substrate was annealed at 75 ℃ to remove residual solvents for 2 minutes under ambient conditions.

Fabrication of the micro-patterned stamp

The preparation of stamp starts with designing the pattern to print red, green, and blue pixels on the substrate (Fig. S10b). The lines and spaces were designed using AutoCAD software to produce glass photomask for photolithography process, and the mask was used for creating master mold that can be used for multiple production of stamps. A cleaned 4-inch Si wafer was

used for photolithography using negative photoresist (SU-8 2010, Microchem) and a developer. After development process, 10 μm thickness of microstructure SU-8 molds have been created to make stamps.

A polydimethylsiloxane (PDMS) (Sylgard 184, Dow) and curing agent have been fully mixed in ratio of 10:1. The 65 g of PDMS is poured onto mold in the square petri dish of 10×10 cm^2 size. The square petri dish containing the PDMS is placed on the stabilizer for 24 hours in ambient condition and moved to the oven at 55 ℃ for 24 hours. Finally, the PDMS stamp is removed from the mold, and patterned stamp in the middle section is used for the transfer printing process.

RGB pixelated QD-LEDs fabrication via the transfer printing process

The overall transfer printing process consists of the preparation of donor substrate, PDMS stamp, patterned ITO substrate for smart white lighting QD-LEDs (Fig. S10). Patterned ITO substrate with PEDOT and TFB layers is a targeted substrate to transfer red, green, and blue layer from the donor substrate. Figure S11 shows the transfer printing equipment used for patterning QD layers in this study. Micro-patterned PDMS stamp was placed on transfer printer and gradually brought down to the QD-coated donor substrate. When the pressing reach 0.5 kg, the stage held 5 seconds, and then picked-up the layer with the speed of 200 mm s^{-1} (Fig. S12a). The PDMS stamp with QD layers brought down to the targeted substrate until embossing 2 kg for 30 seconds, and then removed the stamp slowly in speed of 0.01 mm s^{-1} to transfer pixelated RGB QD layers (Fig. S12b). The samples with PEDOT, TFB, and pixelated QD layers has been annealed 75 ℃ for 5 minutes to enhance adhesions of interface between QD and HTL.

Characterization of QDs and the devices

PL spectra were measured by a spectrofluorometer coupled with an integration sphere (Hamamatsu, Quantaurus-QY plus). The range of wavelength is from 350 nm to 1100 nm which covers the visible light range. The optical properties including EL spectra and current density-luminance-voltage (*J-L-V*) characteristics were measured in an integrating sphere using Photonic Multi-channel Analyzer PMA-12 (Hamamatsu Photonics K.K.) coupled with a source meter (Keithley 2400) for voltage and current source unit.

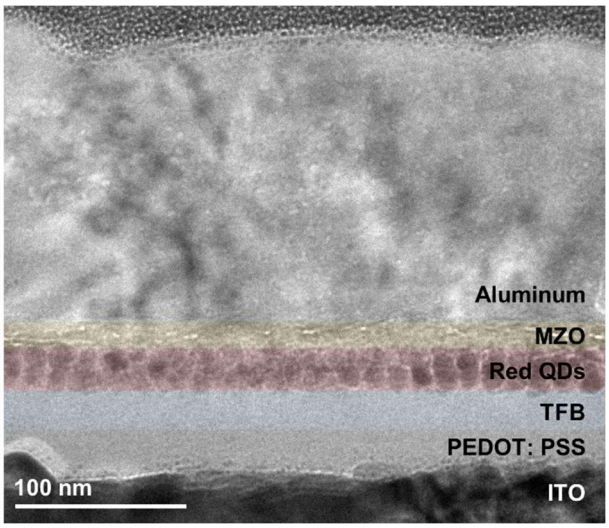

Fig. S1. Cross-sectional TEM image of the red QD-LED device fabricated by the transfer-printing method.

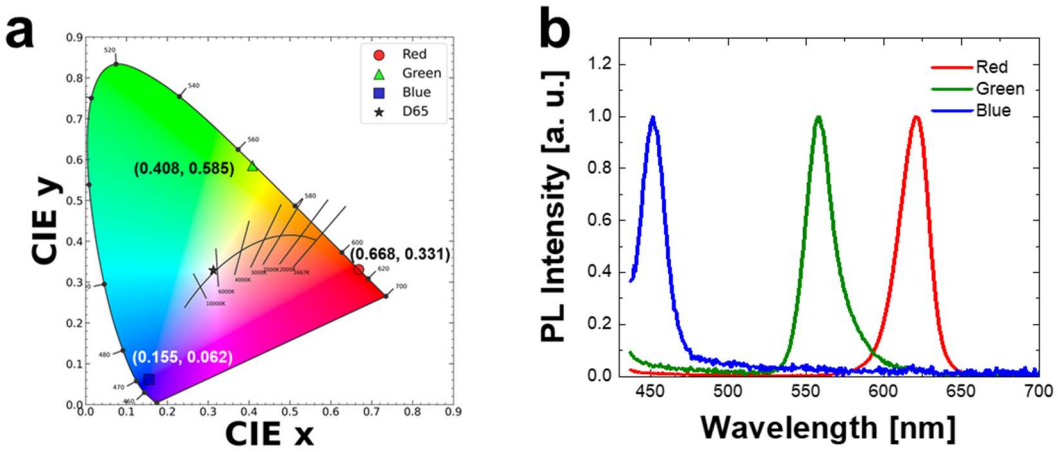

Fig. S2. Color properties of the individual R, G, and B QDs and their monochromatic devices. a) Experimental CIE color coordinates of the R, G, B QD-LEDs obtained from the device fabrication for the patterned-type white QD-LED device. b) Normalized PL spectra of R (620 nm), G (558 nm) and B (450 nm) QDs used for the simulation of the patterned-type QD-LED device.

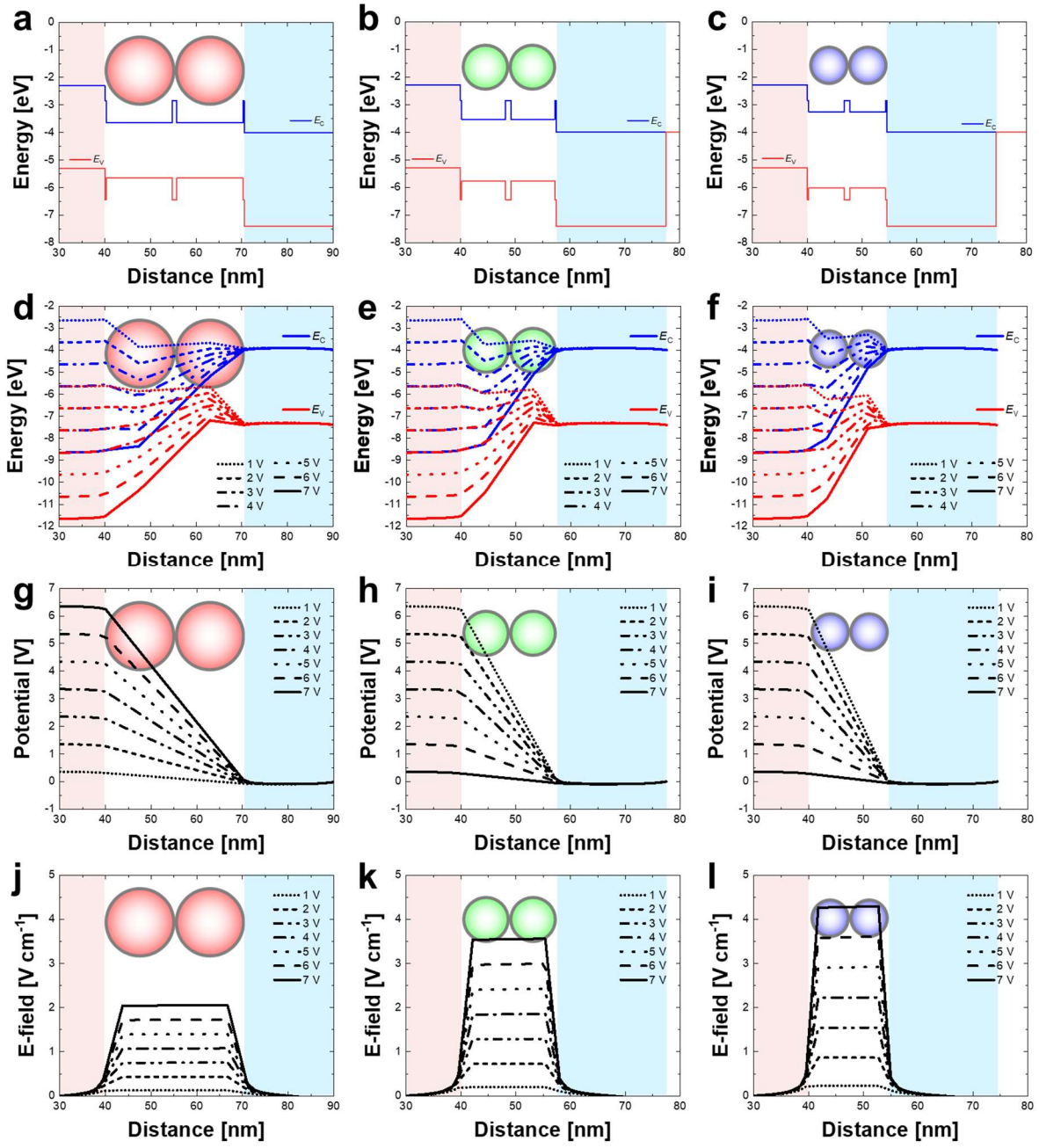

Fig. S3. Energy-levels, potential and electric-field distribution of the simulated monochromatic R, G, and B QD-LED devices used for the optimization of the patterned-type QD-LED with respect to the distance from the interface between anode and HTL. Flat-band energy-levels of conduction and valence bands of a) R, b) G, c) B QD-LED devices. Simulated conduction and valence band energy-level distributions of d) R, e) G and f) B QD-LED devices. Simulated potential distributions of g) R, h) G and i) B QD-LED devices. Simulated electric-field distributions of j) R, k) G and l) B QD-LED devices.

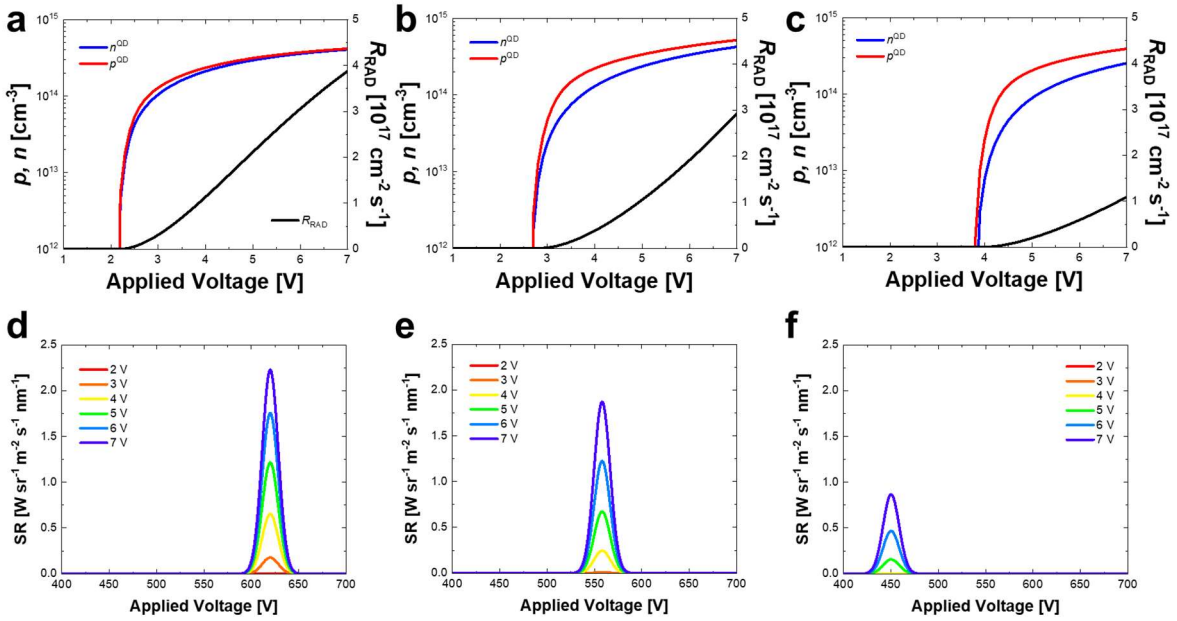

Fig. S4. Hole and electron density accumulated at QD layer and the radiative recombination rates per unit area with respect to the applied voltage of monochromatic a) R, b) G, and c) B QD-LED devices used for the optimization of the patterned-type QD-LED. The simulated spectral radiances of the monochromatic d) R, e) G, and f) B QD-LED devices for different applied voltages.

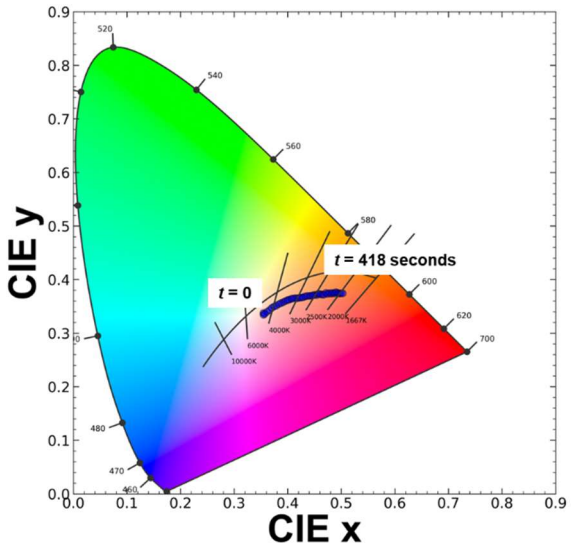

Fig. S5. The time-dependent color shift of the fabricated patterned-type white QD-LED device.

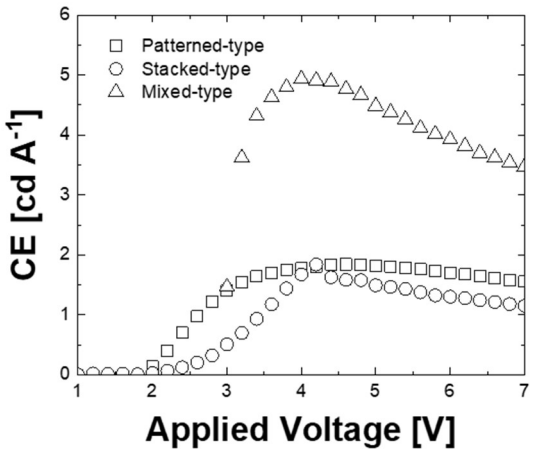

Fig. S6. Current efficiencies of patterned-, stacked-, and mixed-type white QD-LED devices fabricated in this study.

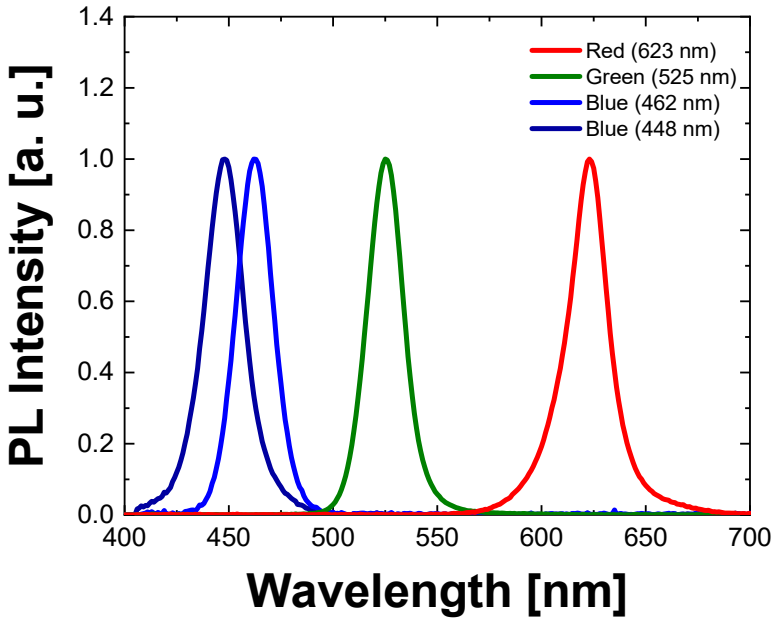

Fig. S7. The optical spectrum of the normalized PL spectra of R (623 nm), G (525 nm) and B (448 nm and 462 nm) QDs used for the fabrication of the stacked- and mixed-type QD-LEDs.

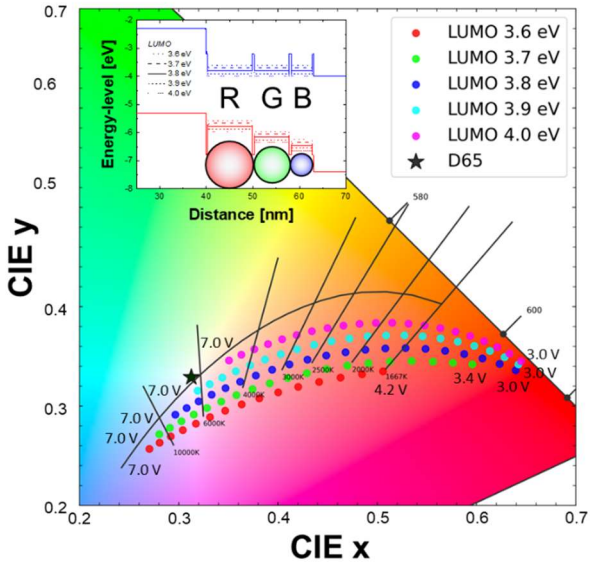

Fig. S8 Color variations of the R/G/B stacked white QD-LED devices with different energy level configurations of QD LUMO from 3.6 eV to 4.0 eV with 0.1 eV step.

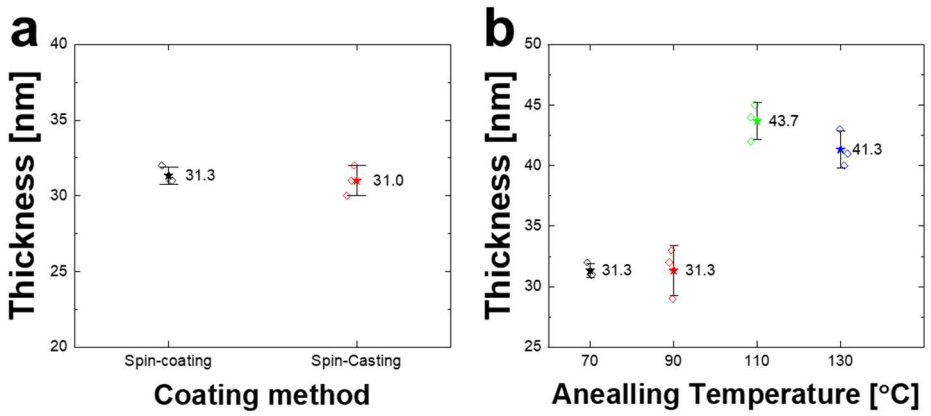

Fig. S9. Thickness of the red QD layer for a) different fabrication methods (spin-coating and spin-casting) and b) different annealing temperatures of 70 ºC, 90 ºC, 110 ºC, and 130 ºC.

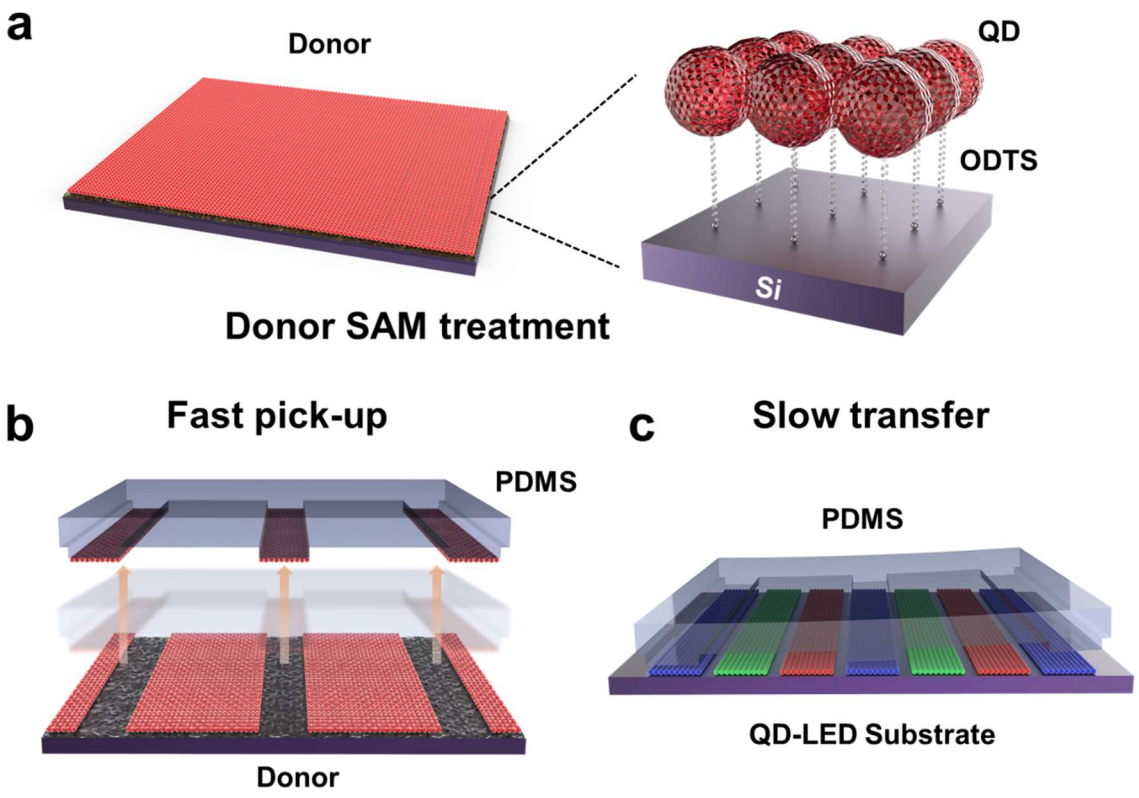

Fig. S10. Transfer printing technology for fabricating the patterned-type QD-LED device. a) QDs on a SAM treated donor substrate. b) Pick-up process and c) transfer printing process by patterned PDMS stamp.

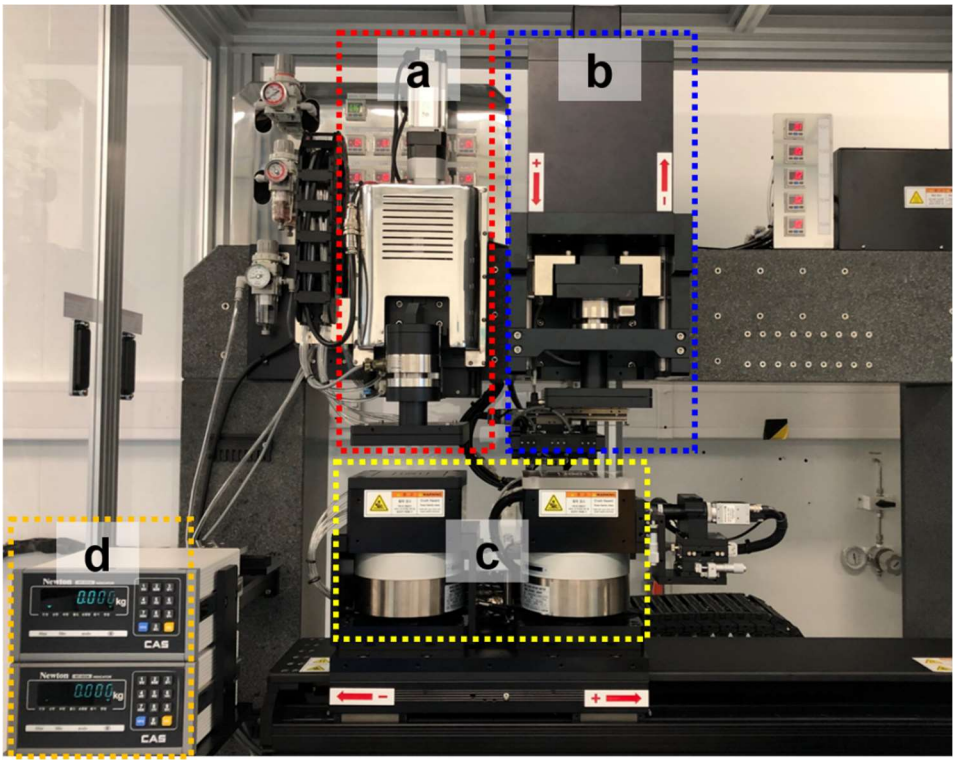

Fig. S11. Snapshot of the transfer printing equipment. a) High speed module with the solenoid pump for the pick-up process. b) Low speed module with linear motor for the transfer process. c) Substrate holder. d) Pressure indicator.

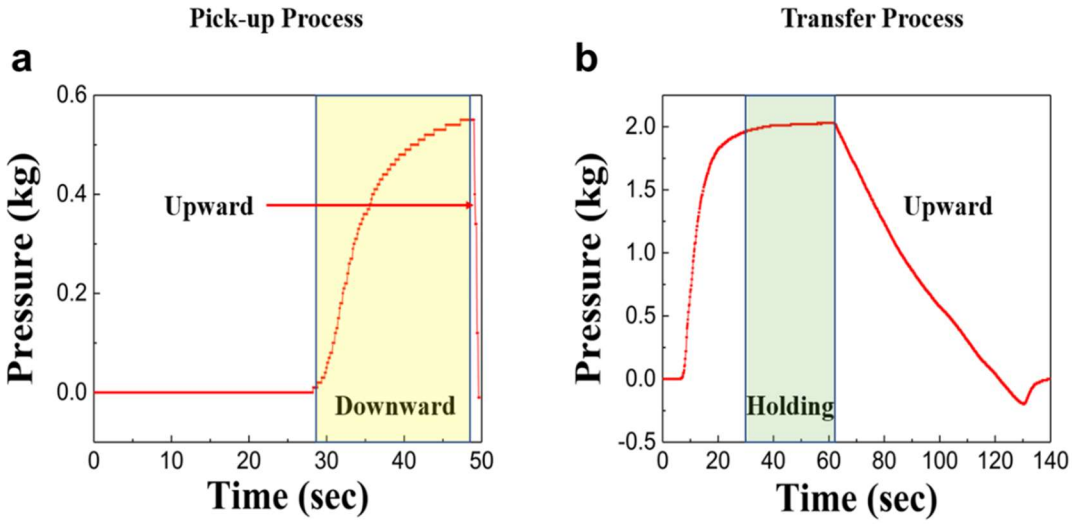

Fig. S12. Pressure as a function of time during a) the pick-up and b) the transfer processes.

Table S1. Material parameters for the transport layers used in the charge transport simulation.

Parameters	Anode	HIL	HTL	ETL	Cathode
Materials	ITO	PEDOT:PSS	TFB	MZO	Al
Thickness [nm]		20	20	20	
Work function [eV]	-4.7	-	-	-	-4.0
LUMO [eV]		-3.60[3]	-2.30[10]	-4.00[11,12]	
HOMO [eV]		-5.17[3]	-5.30[10]	-7.40[11,12]	
Intrinsic carrier concentration n_i [cm^{-3}]		1.6×10^{6}	1.6×10^{-6}	6.9×10^{-10}	
Hole mobility μ_p [$cm^2\ V^{-1}\ s^{-1}$]		3.2×10^{-4}[13]	$2.0e\times10^{-3}$[14]	2.0×10^{-3}[15]	
Electron mobility μ_n [$cm^2\ V^{-1}\ s^{-1}$]		3.2×10^{-4}[13]	$2.0e\times10^{-3}$[14]	2.0×10^{-3}[15]	
Dielectric constant ε_r		3.0[13]	3.5[10]	8.5[11]	
Electron doping density N_d [cm^{-3}]		-	-	1.0×10^{17}[4]	
Hole doping density N_a [cm^{-3}]		2.81×10^{19}[16]	1.0×10^{17}[4]	-	
SRH lifetime τ [μs]		1.0[3,4]	1.0[3,4]	1.0[3,4]	

Table S2. Material parameters for red, green, and blue QDs used in the charge transport simulation of patterned-type QD-LED.

Parameters	QDs			
	Red Core	Green Core	Blue Core	Shell
Materials	CdSe	CdSe	CdSe	ZnS
Dielectric constant ε_r^{QD}	9.4[17]	9.4[17]	9.4[17]	-
Peak wavelength λ_{peak}[nm]	620	558	450	-
FWHM, $\Delta\lambda$ [nm]	20	20	20	-
Diameter d_{QD} [nm]	15.0	8.5	7.0	-
Number of QD layers	2	2	2	-
LUMO [eV]	-3.65	-3.54	-3.27	-2.85
Optical bandgap [eV]	2.00	2.22	2.72	3.60
Intrinsic carrier concentration n_i [cm^{-3}]	399	5.5	1.8×10^{-4}	
Hole capturing volume α_p [cm^3]	5.71×10^{-18}	1.71×10^{-19}	5.39×10^{-20}	-
Electron capturing volume α_n [cm^3]	5.71×10^{-18}	1.71×10^{-19}	5.39×10^{-20}	-
PLQY of QD η_{QD}	0.6	0.6	0.6	-
Langevin strength γ [$cm^3\ s^{-1}$]	1.0×10^{-12}	1.0×10^{-12}	1.0×10^{-12}	-
SRH lifetime τ [μs]	7.79	1.27	0.49	-
Auger probability C [$cm^6\ s^{-1}$]	9.14×10^{-31}	5.65×10^{-30}	1.59×10^{-29}	-

Table S3. Summary of the device EL and color performances reported from the different types of Cd-based white QD-LEDs.

Publications	Device features	EQE [%]	Current efficiency (CE) [cd/A]	CIE_{xy} (@ white)	CCT [K]
This work	**Patterned White**	**0.6**	**1.8**	**(0.31, 0.33)**	**2,998 – >10,000**
	Stacked White	**0.8**	**1.4**	**(0.32, 0.28)**	**2,244 – >10,000**
	Mixed White	**2.0**	**3.9**	**(0.31, 0.28)**	**3,694 – 8,955**
Bae *et al*.[18]	Mixed White (Spin-coated)	0.9	-	(0.31, 0.32)	6,874
Hames *et al*.[19]	Mixed White (Spin-coated)	0.2	0.5	-	7,265
Anikeeva *et al*.[20]	Mixed White (Spin-coated)	0.3	0.7	(0.35, 0.41)	5,500
Lee *et al*.[21]	Stacked White (Spin-coated)	3.1	7.7	(0.32, 0.33)	-
Kim *et al*.[22]	Stacked White (Transfer-printed)	-	0.4	(0.36, 0.37)	-
Choi *et al*.[23]	Patterned White (Transfer-printed)	1.6	-	(0.39, 0.38)	-

Supplementary References

1 S.-M. Jung, T. H. Lee, S. Y. Bang, S. D. Han, D.-W. Shin, S. Lee, H. W. Choi, Y.-H. Suh, X.-B. Fan, J.-W. Jo, S. Zhan, J. Yang, C. Samarakoon, Y. Kim, L. G. Occhipinti, G. Amaratunga and J. M. Kim, *npj Comput. Mater.*, 2021, **7**, 122.

2 V. P. Sirkeli, O. Yilmazoglu, F. Küppers and H. L. Hartnagel, *Semicond. Sci. Tech.*, 2015, **30**, 065005.

3 F. Vahabzad, A. Rostami, M. Dolatyari, G. Rostami and I. S. Amiri, *Physica B*, 2019, **574**, 411667.

4 B. Kumar, S. A. Campbell and P. Paul Ruden, *J. Appl. Phys.*, 2013, **114**, 044507.

5 C. Fazio, O. R. Battaglia and I. Guastella, *Eur. J. Phys.*, 2012, **33**, 359–371.

6 U. K. Verma and B. Kumar, *J. Appl. Phys.*, 2017, **122**, 153104.

7 C. Liang, Y. Wang, D. Li, X. Ji, F. Zhang and Z. He, *Sol. Energy Mater. Sol. Cells*, 2014, **127**, 67–86.

8 W. H. Press, Ed., *Numerical recipes in C: the art of scientific computing*, Cambridge University Press, Cambridge ; New York, 2nd ed., 1992.

9 S. Jung, H. W. Choi, F. C. Mocanu, D.-W. Shin, M. F. Chowdhury, S. D. Han, Y.-H. Suh, Y. Cho, H. Lee, X. Fan, S. Y. Bang, S. Zhan, J. Yang, B. Hou, Y. T. Chun, S. Lee, L. G. Occhipinti and J. M. Kim, *Sci Rep*, 2019, **9**, 20376.

10 Y. J. Han, K. An, K. T. Kang, B.-K. Ju and K. H. Cho, *Sci. Rep.*, 2019, **9**, 10385.

11 S. Vallisree, R. Thangavel and T. R. Lenka, *Mater. Res. Express*, 2018, **6**, 025910.

12 J. Kim, J.-H. Yun, C. H. Kim, Y. C. Park, J. Y. Woo, J. Park, J.-H. Lee, J. Yi and C.-S. Han, *Nanotechnology*, 2010, **21**, 115205.

13 B. Xu, S.-A. Gopalan, A.-I. Gopalan, N. Muthuchamy, K.-P. Lee, J.-S. Lee, Y. Jiang, S.-W. Lee, S.-W. Kim, J.-S. Kim, H.-M. Jeong, J.-B. Kwon, J.-H. Bae and S.-W. Kang, *Sci. Rep.*, 2017, **7**, 45079.

14 Y. Zhao, L. Chen, J. Wu, X. Tan, Z. Xiong and Y. Lei, *IEEE Electron Device Lett.*, 2020, **41**, 80–83.

15 F. Wang, W. Sun, P. Liu, Z. Wang, J. Zhang, J. Wei, Y. Li, T. Hayat, A. Alsaedi and Z. Tan, *J. Phys. Chem. Lett.*, 2019, **10**, 960–965.

16 F. Yan, E. P. J. Parrott, B. S.-Y. Ung and E. Pickwell-MacPherson, *J. Phys. Chem. C*, 2015, **119**, 6813–6818.

17 C. Canali, F. Nava, G. Ottaviani and C. Paorici, *Solid State Communications*, 1972, **11**, 105–107.

18 W. K. Bae, J. Lim, D. Lee, M. Park, H. Lee, J. Kwak, K. Char, C. Lee and S. Lee, *Adv. Mater.*, 2014, **26**, 6387–6393.

19 B. C. Hames, I. Mora-Seró and R. S. Sánchez, *Nano Res.*, 2018, **11**, 1575–1588.

20 P. O. Anikeeva, J. E. Halpert, M. G. Bawendi and V. Bulović, *Nano Lett.*, 2007, **7**, 2196–2200.

21 K.-H. Lee, C.-Y. Han, E.-P. Jang, J.-H. Jo, S. Hong, J. Y. Hwang, E. Choi, J.-H. Hwang and H. Yang, *Nanoscale*, 2018, **10**, 6300–6305.

22 T.-H. Kim, D.-Y. Chung, J. Ku, I. Song, S. Sul, D.-H. Kim, K.-S. Cho, B. L. Choi, J. Min Kim, S. Hwang and K. Kim, *Nat. Commun.*, 2013, **4**, 2637.

23 M. K. Choi, J. Yang, K. Kang, D. C. Kim, C. Choi, C. Park, S. J. Kim, S. I. Chae, T.-H. Kim, J. H. Kim, T. Hyeon and D.-H. Kim, *Nat. Commun.*, 2015, **6**, 7149.